Journal of Nuclear Materials 381 (2008) 259–266

Contents lists available at ScienceDirect

Journal of Nuclear Materials

journal homepage: www.elsevier.com/locate/jnucmat

Light ion irradiation-induced phase transformation in the monoclinic polymorph of zirconia

James A. Valdez [a,*], Zhenhuan Chi [b], Kurt E. Sickafus [a]

[a] Materials Science and Technology Division, Los Alamos National Laboratory, Mail-Stop G755, Los Alamos, NM 87545, USA
[b] Renishaw Inc., 5277 Trillium Blvd., Hoffman Estates, IL 60192, USA

ARTICLE INFO

Article history:
Received 1 May 2007
Accepted 18 July 2008

PACS:
61.80.Jh
81.05.Je
61.82.Ms
61.16.Bg
61.80.Az
61.14.Lj
61.10.Kw
64.60.My
78.30.−j

ABSTRACT

Ion irradiation damage experiments were performed at ~80 K on polycrystalline samples of monoclinic, slightly sub-stoichiometric zirconia ($ZrO_{1.98}$). Following irradiation with 150 keV Ne^+ ions, the monoclinic phase was gradually replaced by a new phase. Transmission electron microscopy (TEM) observations in cross-sectional geometry and electron microdiffraction (μD) measurements revealed that the irradiated layer in a sample irradiated to a fluence of 5×10^{20} Ne/m^2 is partially transformed to a higher symmetry phase of high crystallinity. This phase transformation is accompanied by reduction of the initial micron-sized, highly-twinned grain distribution, to a nano-phased grain structure. Grazing incidence X-ray diffraction (GIXRD) measurements revealed that the radiation-induced phase is a tetragonal polymorph of zirconia. This was verified by the existence of strong (101) diffraction maxima and weak (102) reflections (body-centered cell). Raman spectroscopy (RS) measurements were also performed in an attempt to corroborate GIXRD results obtained from the irradiated material. RS measurements in the confocal geometry agreed with GIXRD measurements, although RS was not as definitive as GIXRD. In addition to RS showing the existence of a band corresponding to a tetragonal structure at 262 cm^{-1}, a new mystery band appeared at 702 cm^{-1} that increased in intensity as a function of irradiation fluence.

1. Introduction

Zirconia (zirconium dioxide, nominally with stoichiometry ZrO_2) has long attracted the interest of scientists and engineers because of its important ceramic properties. It is one of the most refractory of all oxide compounds and it exhibits both high thermal shock and corrosion resistance [1]. Zirconia also exists in three crystallographic modifications as a function of temperature at atmospheric pressure [2]:

$$\text{monoclinic} \overset{1170^\circ C}{\leftrightarrow} \text{tetragonal} \overset{2370^\circ C}{\leftrightarrow} \text{cubic} \overset{2680^\circ C}{\leftrightarrow} \text{liquid}$$

The tetragonal-to-monoclinic transformation shown above has been exploited in ZrO_2-containing ceramics that are 'transformation toughened' [3].

The monoclinic phase of zirconia (m-ZrO_2) is often referred to by its mineralogical name, baddeleyite, and belongs to space group $P2_1/c$ (S.G. # 14). Tetragonal zirconia (t-ZrO_2) is described in the literature using either a body-centered tetragonal (*bct*) or face-centered tetragonal (*fct*) unit cell. In this paper, we will adopt the bct description (Fig. 1). The space group for t-ZrO_2 is $P4_2/nmc$ (S.G. # 137) with Zr atoms occupying the 2*a* Wyckoff equipoint and O atoms occupying the 4*d* equipoint in the 1st setting for this space group. The structure of t-ZrO_2 was first refined by Teufer [4] and has come to be known as the 'Teufer' structure for tetragonal phase ZrO_2.

Several recent radiation damage studies of zirconia have revealed that polymorphism plays a significant role in the radiation damage evolution of ZrO_2. Sickafus et al. [5] found, based on transmission electron microscopy observations, that monoclinic zirconia (m-ZrO_2) exposed to 340 keV Xe^{++} ions (in the nuclear stopping energy regime) at 120 K, transformed to a higher symmetry phase, either t-ZrO_2 or cubic (c-ZrO_2), by a peak displacement damage dose between 2 and 20 displacements per atom (dpa). This crystalline phase was reported to resist further transformation (especially amorphization) to a peak dose of more than 100 dpa [5–6]. Simeone et al. [7] observed a similar transformation of m-ZrO_2 to the t-ZrO_2 polymorph (heretofore denoted as an m–t transformation), under primarily nuclear stopping conditions using 800 keV Bi ions. Simeone et al. [7] used X-ray diffraction to reveal the m–t transformation, by observing the emergence of a $(101)_t$ reflection with increasing Bi^+ dose. It should be noted, however, that this reflection can also be indexed as a $(111)_c$ reflection from a cubic c-ZrO_2 phase. Simeone et al. [7] employed Raman spectroscopy to eliminate this ambiguity and identified a small spectral feature at ~257 cm^{-1}, which can only be attributed to t-ZrO_2. Valdez et al. [8] demonstrated that 300 keV Kr^{++} ion irradiation of m-ZrO_2 also produces

* Corresponding author. Tel.: +1 505 665 3034; fax: +1 505 667 8601.
E-mail address: javaldez@lanl.gov (J.A. Valdez).

0022-3115/$ - see front matter © 2008 Elsevier B.V. All rights reserved.
doi:10.1016/j.jnucmat.2008.07.045

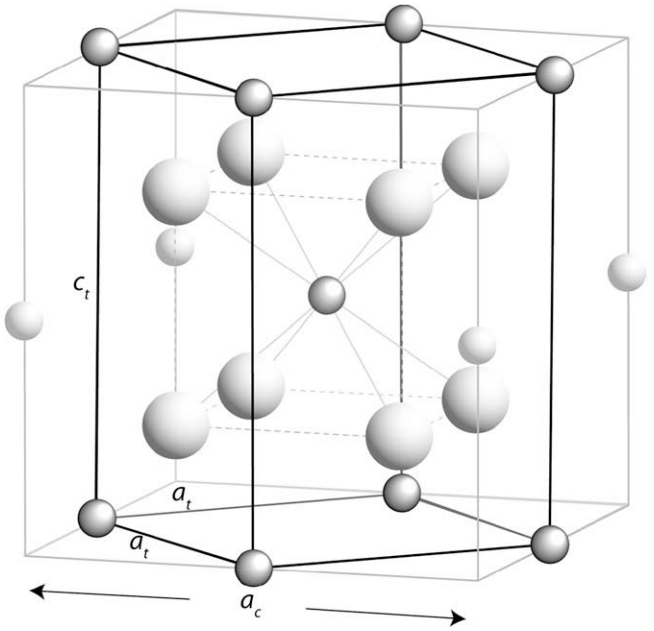

Fig. 1. Schematic diagrams illustrating the relationship between the body-centered tetragonal (bct) and cubic (*c*) unit cells of ZrO_2. The atoms are shown in their ideal positions for a structure with cubic symmetry. The large spheres represent O anions; the small spheres represent Zr cations. The larger cubic unit cell is translated so that the cations appear 'edge-centered' with respect to the cube edges.

the *m*–*t* transformation (this is in primarily a nuclear stopping regime). This phase change was characterized by Valdez et al. [8] using three characterization techniques, namely confocal Raman spectroscopy, grazing incidence X-ray diffraction and cross-sectional transmission electron microscopy. In other experiments using swift heavy ions (135 MeV ^{58}Ni, 300 MeV ^{76}Ge and 250 MeV ^{127}I), where primarily electronic stopping dominates over nuclear stopping, Benyagoub et al. [9–11], observed a similar *m*–*t* ZrO_2 transformation, based on X-ray diffraction and Raman spectroscopy measurements. Most significantly, Benyagoub et al. [9] observed a prominent *t*-ZrO_2 Raman feature at ~265 cm^{-1} in ZrO_2 irradiated with 300 MeV Ge ions.

In this report, we examine radiation damage effects in ZrO_2 induced by noble gas, Ne^+ ions. The purpose of this study is to assess further the sensitivity to spectrum effects of the *m*–*t* transformation observed in previous irradiation damage studies of ZrO_2. The use of light Ne^+ ions allows us to enhance the total ionization loss per unit damage energy, compared to the heavy ion, Kr^+ irradiation experiments that we performed previously [8]. Zinkle [12–14] has shown that irradiation-induced microstructures in oxides such as MgO, Al_2O_3, and $MgAl_2O_4$ are influenced by irradiating ion mass, especially by corresponding variations in electronic-to-nuclear stopping power characteristics of the irradiation spectrum. In particular, enhanced electronic stopping was shown to suppress dislocation loop nucleation, while at the same time enhancing loop growth [12–14]. These effects were attributed to ionization-induced diffusion of point defects in these oxides [15]. The experimental results presented here will be examined for evidence of similar irradiation spectrum effects.

2. Experimental procedure

ZrO_2 powders supplied by CERAC Corp. (99.995% pure, 325 mesh) were hot-pressed in a graphite die at 24 MPa for 2.5 h at 2070 K. Hot-pressed sample densities were estimated geometrically to be ~98% of the theoretical value. Samples cut from the hot-pressed pucks were uniform black in color. The black color is usually indicative of oxygen deficiency. Thermal gravimetric analysis (TGA) revealed the stoichiometry to be $ZrO_{1.98}$. Sample wafers were polished using 0.25 μm diamond impregnated lapping films to a mirror finish. A typical wafer dimension was $10 \times 10 \times 0.5$ mm. X-ray diffraction indicated that the as-prepared zirconia samples were nearly phase pure and possessed the monoclinic, baddeleyite structure. Analysis of the diffraction data revealed further that the monoclinic lattice parameters of the 'ZrO_2' are a = .5153 ± 5 nm, b = .5193 ± 5 nm, c = .5343 ± 5 nm, β = 99° 38' ± 10', and the molecular volume is V_{mol} = 0.0352 nm^3/ZrO_2. This compares favorably with, for instance, refinement of high resolution neutron powder diffraction data obtained by Howard et al. [16] (also JCPDF file #78-1807 [17]) where the lattice parameters of *m*-ZrO_2 were found to be a = .51505(1) nm, b = .52116(1) nm, c = .53173(1) nm, β = 99.230(1)°, which yields a molecular volume of V_{mol} = 0.0352 nm^3/ZrO_2. In addition, a *t*-ZrO_2 specimen was also prepared using co-precipitation procedures. The *t*-ZrO_2 phase was stabilized using 12 mol% Ce. This specimen was used as a standard for Raman spectroscopy measurements.

Zirconia samples were irradiated with 150 keV Ne^+ ions in the Ion Beam Materials Laboratory at Los Alamos National Laboratory using a 200 kV Varian implanter. Ion fluences ranged from 5×10^{19} to 1×10^{21} Ne/m^2. This fluence range was chosen to achieve similar displacement damage doses to those used in previous irradiation experiments performed by Valdez et al. using Kr^{++} ions [8]. All irradiations were performed using a liquid nitrogen-cooled specimen holder (sample temperature ~80 K) and using a constant ion flux of 1×10^{16} Ne/m^2 s (ion flux was kept as low as practically possible, in order to minimize sample heating effects). Fig. 2 shows characteristics of the 150 keV Ne^+ ion implantation into *m*-ZrO_2, obtained using the Monte Carlo ion transport code SRIM2000 [18] (displacement energies of 40 eV for Zr and O atoms and a density of 8.8 gm/cm^3 were used for these calculations). Fig. 2(a) shows estimates of energy loss partitioned into nuclear and electronic components for 150 keV Ne in *m*-ZrO_2. Fig. 2(b) shows estimates of ballistic damage (in units of dpa) and implanted Ne atomic concentration as a function of depth into the target, for the highest fluence of 1×10^{21} Ne/m^2 used in these experiments.

Ion irradiation-induced damage was assessed using three materials characterization techniques: (1) transmission electron microscopy (TEM); (2) grazing incidence X-ray diffraction (GIXRD); and (3) Raman spectroscopy (RS). TEM observations were made using a Philips CM-30 instrument operating at 300 kV. GIXRD measurements were made using a Bruker AXS D8 Advance X-ray diffractometer, Cu K_α radiation, and θ–2θ geometry. The X-ray diffractometer was equipped with a Göebel mirror to achieve parallel beam diffraction optics. The θ–2θ scans were performed using a step size of 0.008° and a dwell time of 1 s per step unless indicated otherwise. Three grazing angles of incidence, γ = 0.25°, 0.5° and, 1.0°, were used for GIXRD measurements, in such a way that the calculated X-ray penetration depths fell within the range of the implanted Ne^+ ions in the ZrO_2 target material. X-ray penetration depths can be estimated both geometrically (see, e.g., Rafaja et al. [19]) and based on critical angle, total external reflection (see, e.g., Guinier [20] and Lim [21]). Geometrically, the GIXRD penetration depth is given by $\sin(\gamma)\sin(2\theta-\gamma) / \mu(\sin(\gamma)+\sin(2\theta-\gamma))$, where γ is the X-ray angle of incidence, 2θ is the diffraction angle for the particular measurement, and μ = 620 cm^{-1} is the linear absorption coefficient for ZrO_2. In terms of the critical angle for external reflection, α_c, the GIXRD penetration depth is given by $\lambda/2\pi(\alpha_c^2 - \gamma^2)^{\frac{1}{2}}$ for $\gamma < \alpha_c$, and by $2\ \gamma/\mu$ for $\gamma > \alpha_c$, where λ is the X-ray wavelength and $\alpha_c \cong \sqrt{2\,\delta} = 1.6 \times 10^{-3}\sqrt{\rho}\,\lambda$, where $\delta = (1-\eta)$ for refractive index, η (ρ is the density of the material in gm cm^{-3} and λ is the X-ray wavelength in Å). Fig. 3 shows plots of GIXRD X-ray penetration in ZrO_2, based on these two methods of

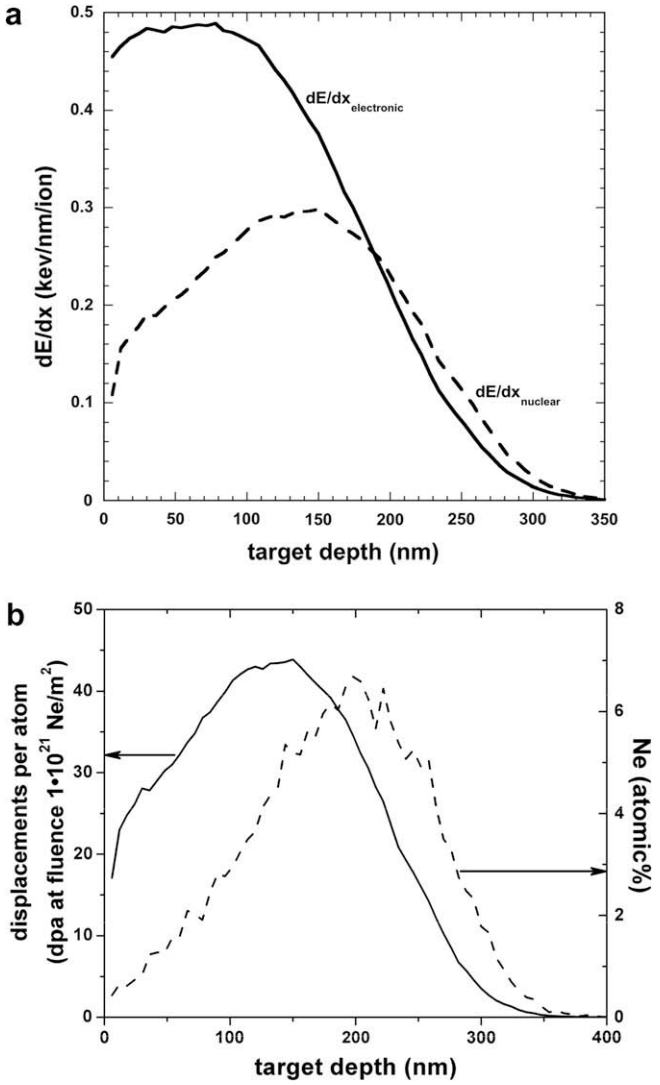

Fig. 2. SRIM simulation results for 150 keV Ne^+ ion irradiation of ZrO_2. (a) Energy loss as a function of depth for the nuclear and electronic stopping components of the stopping power (energy partitioning includes both primary and secondary knock-on effects). (b) Displacement damage (left-hand ordinate) and implanted Ne^+ ion concentration (right-hand ordinate) as a function of depth for Ne^+ ion irradiation of ZrO_2 to a fluence of 1×10^{21} Ne/m^2.

calculation. Comparing Figs. 2(b) and 3, it is clear that GIXRD patterns obtained with $\gamma = 0.25^\circ$ probe the uppermost portion of the implanted layer, patterns obtained with $\gamma = 0.5^\circ$ probe from the surface to the maximum in the displacement damage profile and possibly beyond, and patterns obtained with $\gamma = 1.0^\circ$ probe the entire implanted region, in addition (perhaps) to some unirradiated substrate material. To keep effects from the implanted Ne^+ and unirradiated substrate material and to a minimum, GIXRD measurement results discussed later were all collected using the grazing incidence angle of $\gamma = 0.25^\circ$.

RS measurements were obtained using a confocal Renishaw Raman Microprobe 1000. A 488 nm wavelength excitation at 3 mW of power was used (argon ion laser) and a count time of 10 s at focus with a 50× objective lens.

3. Results

Fig. 4 shows a bright-field TEM micrograph obtained in cross-sectional geometry from m-ZrO_2 irradiated with 150 keV Ne^+ ions to a fluence of 5×10^{20} Ne/m^2. The area imaged shows a portion

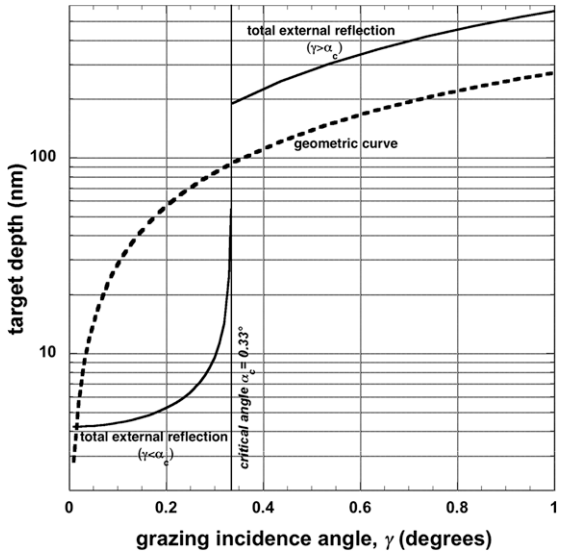

Fig. 3. Grazing incidence X-ray diffraction (GIXRD) X-ray penetration depth versus grazing incidence angle (γ), calculated using two different methods (see text for discussion).

of a single grain in the unirradiated substrate along with several twins (twins are expected for monoclinic zirconia processed under our sintering conditions). The thickness of the irradiated layer in the image is 280 nm, which (surprisingly) is somewhat narrower than the 350 nm predicted by SRIM (Fig. 2). The irradiated layer consists of very fine grains (nano-sized) and diffraction contrast arising from a high concentration of irradiation-induced defects. Fig. 4 also shows microdiffraction patterns (μD) obtained from upper and lower portions of the irradiated layer and from the unirradiated substrate. Indexing of the uppermost diffraction pattern revealed that the upper portion of the irradiated layer consists of both monoclinic and tetragonal ZrO_2 reflections while the bottom of the layer exhibits only tetragonal reflections. The incident beam direction in the lower portion of the irradiated layer is consistent with $\overline{\mathbf{B}} = [111]_t$. The microdiffraction pattern from the substrate can be indexed as a monoclinic structure, with an incident beam direction given by $\overline{\mathbf{B}} = [1\bar{1}0]_m$. We note that our μD results do not establish unambiguously the presence of t-ZrO_2 in the irradiated layer. The μD patterns shown in Fig. 4 can likewise be indexed as arising from a cubic, c-ZrO_2 structure. Additional characterization measurements were performed to resolve this ambiguity.

Fig. 5 shows GIXRD patterns obtained from both unirradiated m-ZrO_2 and ZrO_2 irradiated with 150 keV Ne^+ ions to fluences ranging from 5×10^{19} to 1×10^{21} Ne/m^2. Before irradiation, the principal diffraction maxima in the region of 2θ shown in Fig. 5 are readily indexed as $(11\bar{1})_m$ and $(111)_m$ reflections from m-ZrO_2. Following Ne^+ ion irradiation, the monoclinic peaks are diminished in intensity and a new peak emerges at about $2\theta = 30.25^\circ$. This peak shifts to larger 2θ with increasing ion fluence, indicating a contraction of the lattice planes belonging to this new phase. The appearance of this new peak indicates a change in crystal structure of the irradiated m-ZrO_2. However, this peak can be indexed as either a $(101)_t$ or $(111)_c$ reflection, corresponding to t-ZrO_2 or c-ZrO_2 structures, respectively. GIXRD measurements in this 2θ range do not unambiguously distinguish between such m–t or m–c transformations. This ambiguity has been discussed previously in the literature (see, e.g., Refs. [5,9]). To resolve this uncertainty, we performed GIXRD scans in the angular range from $42^\circ \leqslant 2\theta \leqslant 44^\circ$ in order to assess the presence or absence of a $(102)_t$ reflection. The structure factor for c-ZrO_2 is zero in this angular range. These scans were performed slowly (25 s/step)

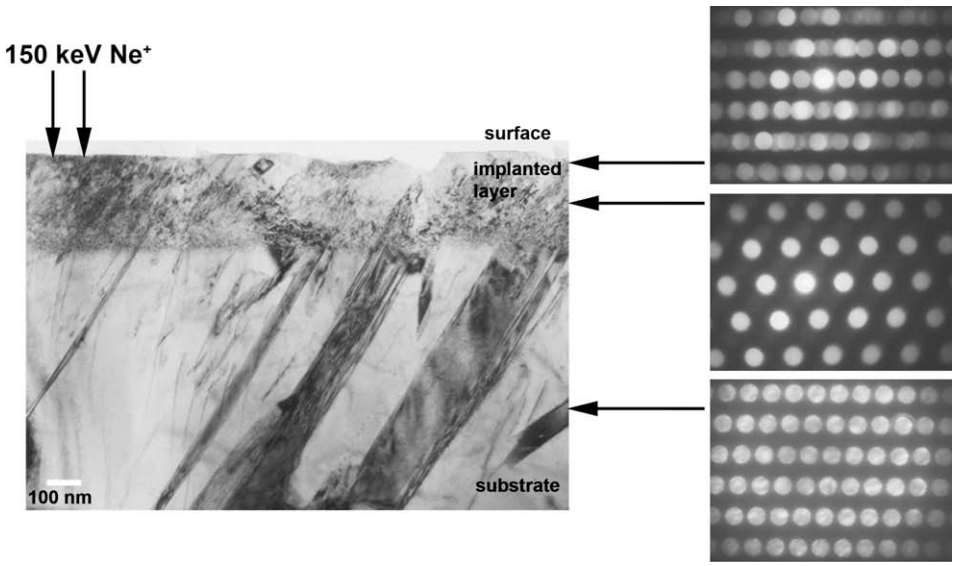

Fig. 4. Bright-field transmission electron microscopy (TEM) micrograph obtained from a cross-sectional sample of ZrO_2 irradiated with 150 keV Ne^+ ions to a fluence of 5×10^{20} Ne/m^2. Also shown are microdiffraction (μD) patterns obtained from small regions (<10 nm diameter) of the ion irradiated layers (top/middle patterns) and the unirradiated substrate (bottom pattern). The incident electron beam direction for the substrate μD pattern is $\overline{\mathbf{B}} = [1\,\bar{1}\,0]_m$.

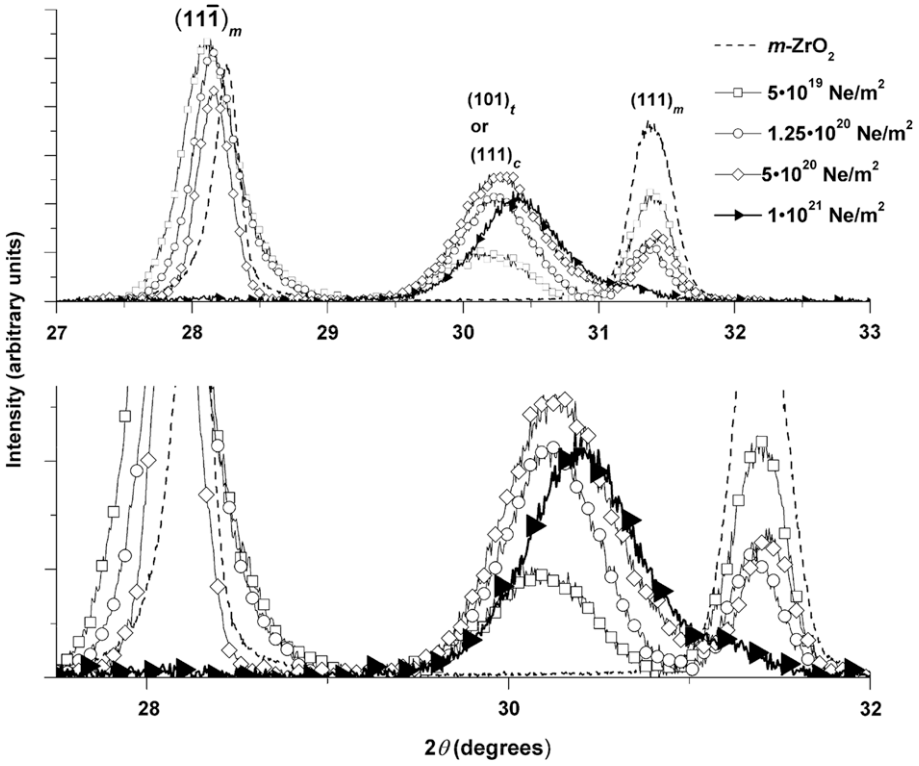

Fig. 5. GIXRD patterns obtained from pristine m-ZrO_2 and ZrO_2 irradiated with 150 keV Ne^+ ions to fluences ranging from 5×10^{19} to 1×10^{21} Ne/m^2. The angle of incidence of the X-ray beam was fixed at $\gamma = 0.25°$. The upper profiles were obtained over the diffraction angular range $27^\circ \leqslant 2\theta \leqslant 33^\circ$. The lower profiles are the same patterns in the range $27.5^\circ \leqslant 2\theta \leqslant 32^\circ$, expanded along the ordinate to emphasize the weaker diffracted intensities.

because the predicted intensity for the $(102)_t$ reflection is extremely small (1% of the 100% t-ZrO_2 peak). Fig. 6 shows GIXRD patterns obtained from unirradiated m-ZrO_2 and ZrO_2 irradiated to a fluence of 1×10^{21} Ne/m^2, using $\gamma = 0.25°$. Unirradiated m-ZrO_2 shows no diffraction features in this range. But in the Ne^+ ion irradiated material, a small peak is apparent at $2\theta \sim 43.2°$. The position of this new peak is consistent with the $(102)_t$ reflection position for t-ZrO_2 reported by Málek et al. [22] and JCPDF file #50-1089 [17] (the latter reference places the $(102)_t$ reflection at $2\theta = 43.140°$ for Cu K_α radiation). Thus, GIXRD provides experimental evidence to support an m–t transformation of ZrO_2 induced by Ne^+ ion irradiation.

The t-ZrO_2 lattice parameters and molecular volume for the highest ion dose used here (fluence 1×10^{21} Ne/m^2) were determined to be $a = 0.3574 \pm 5$ nm, $c = 0.5177 \pm 5$ nm, $V_{mol} = 0.03306$ nm^3/ZrO_2, based on Gaussian curve fits to the observed GIXRD

peaks. These values are in good agreement with those for the tetragonal phase reported by Málek et al. [22] for a metastable, low temperature t-ZrO_2 phase, specifically, a = 0.35984(5) nm, c = 0.5152(1) nm, V_{mol} = 0.03335 nm^3/ZrO_2. Differences may be attributed both to differences in sample stoichiometry and to stresses induced in the irradiated sample surface layers in these experiments.

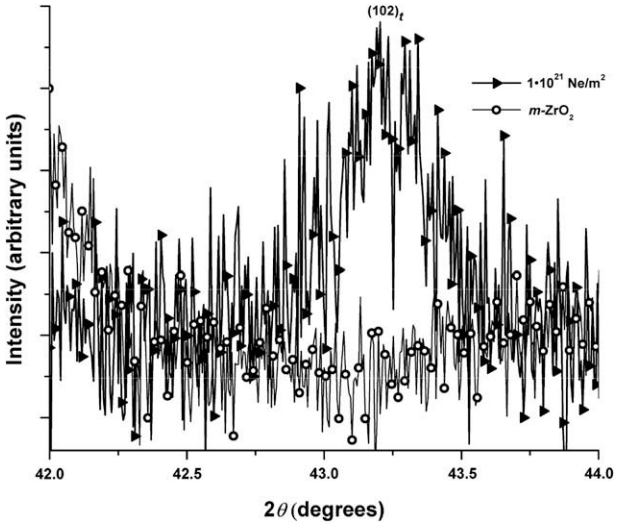

Fig. 6. GIXRD patterns obtained from pristine m-ZrO_2 and ZrO_2 irradiated with 150 keV Ne^+ ions to a fluence of 1 × 1021 Ne/m2. The patterns show the diffraction angular range $42^\circ \leqslant 2\theta \leqslant 44^\circ$. The angle of incidence of the X-ray beam was fixed at $\gamma = 0.25^\circ$. Scan obtained using a dwell time of 25 s per step.

Fig. 7 shows RS spectra obtained from both m-ZrO_2, t-ZrO_2, and ZrO_2 irradiated with Ne^+ ions to fluences ranging from 5×10^{19} to 1×10^{21} Ne/m^2. Fig. 7(a) shows RS spectra obtained from a pristine m-ZrO_2 sample and from a Ce-stabilized, t-ZrO_2 standard specimen. Fig. 7(b) shows RS data obtained from ZrO_2 irradiated with Ne^+ ions to successively higher fluences. The irradiated RS spectra in Fig. 7(b) show the gradual appearance of a faint band at ~262 cm^{-1}, a band not present in the RS spectrum obtained from the unirradiated sample. With increasing Ne^+ ion fluence, this peak increases in resolution and intensity. This Raman shift position corresponds well with the most intense band in the RS spectrum obtained from the Ce-stabilized t-ZrO_2 control sample (Fig. 7(a)). This faint band was previously observed in ion irradiated ZrO_2 samples [7–9] and was attributed to a tetragonal zirconia phase produced by ion irradiation.

Another RS band centered at 702 cm^{-1} also grows in intensity with increasing Ne^+ ion fluence (Fig. 7(b)). Comparing the RS standard spectra (Fig. 7(a)) to the irradiated RS spectra (Fig. 7(b)), it is clear that there are no bands belonging to either m-ZrO_2 or t-ZrO_2 coinciding with the position of this new band. It is interesting to note that we also observed this same band with similar shape and intensity in an RS spectrum obtained from a ZrO_2 sample irra-

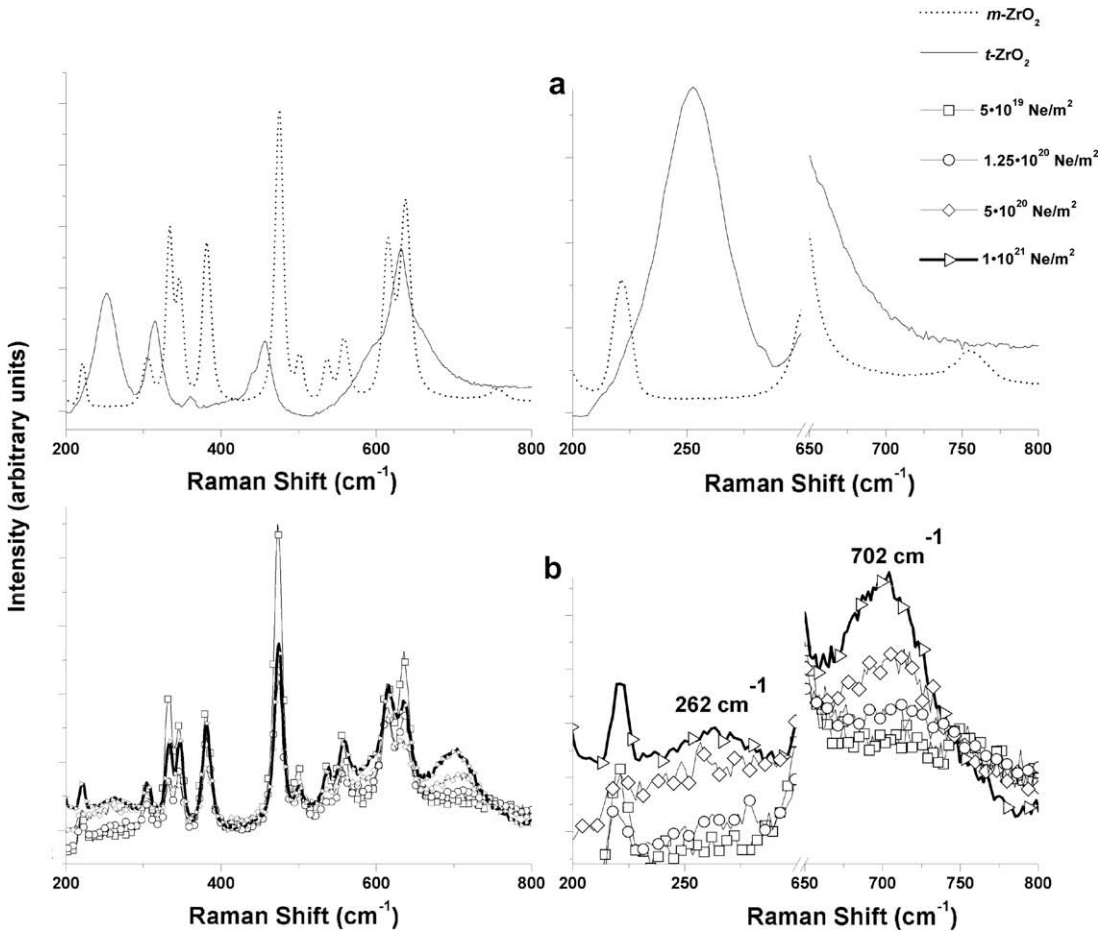

Fig. 7. **(a)** Raman spectroscopy (RS) spectra obtained from pristine m-ZrO_2 (dotted line) and from a Ce-stabilized, t-ZrO_2 standard specimen (solid line). Spectra on the right are the same as those on the left, but expanded along the ordinate to enhance details of weaker RS features. **(b)** RS spectra obtained from ZrO_2 irradiated with 150 keV Ne^+ ions over a fluence range of 5×10^{19}–1×10^{21} Ne/m^2. Spectra shown on the right are the same as those shown on the left, with the ordinate expanded to show additional details in the smaller RS bands. Two new bands appear at ~262 and ~702 cm^{-1} following ion irradiation.

diated with 300 keV Kr^{++} ions to a fluence of 1×10^{20} Kr/m^2 (data not shown here; sample from the study in Ref. [8]). This new band may be due to another phase of zirconia. To test this hypothesis, we also acquired an RS spectrum from a sample of yttria-stabilized cubic zirconia, but we observed no features in the spectral vicinity of 700 cm^{-1} (data not shown). We are continuing to investigate the origin of this mystery RS band.

4. Discussion

Based on the results presented here, we conclude that m-ZrO_2 undergoes a monoclinic-to-tetragonal, m–t transformation to a t-ZrO_2 phase when irradiated with 150 keV Ne^+ ions at cryogenic temperature. The m–t transformation found here is consistent with findings in several previous ion irradiation damage studies [7–11]. In addition, the new tetragonal phase is very stable, based on GIXRD measurements taken 550 days after Ne^+ ion irradiations. GIXRD patterns on aged specimens also showed almost no change in either t-ZrO_2 phase concentration or molecular volume.

Fig. 8 shows results of an attempt to estimate the Ne^+ ion-induced m–t transformation rate, based on GIXRD results presented in the previous section (using X-ray incidence angle, $\gamma = 0.25°$). In Fig. 8, the percentage of m-ZrO_2 transformed to t-ZrO_2 (t%) was estimated using the following formula from Garvie and Nicholson [23]: $t\% = I(101)_t/(I(111)_m + I(111)_m + I(101)_t)$, where I represents the integrated peak area for a specific reflection. These calculations suggest that the tetragonal phase transformation progressed to a maximum of approximately 85% at the maximum experimental fluence of 1×10^{21} Ne/m^2. Fig. 8 also shows that the d-spacing belonging to the $(101)_t$ family of t-ZrO_2 planes decreases with increasing Ne^+ fluence, with a measured contraction of ~0.72% by the maximum fluence of 1×10^{21} Ne/m^2. We speculate that higher doses may lead to further volume contraction, such that the material approaches a structure indistinguishable from a cubic fluorite (c-ZrO_2).

Interestingly, the rate of transformation from m-ZrO_2 to t-ZrO_2 observed in these Ne^+ ion irradiation experiments is slower compared to our previously published Kr^+ ion irradiation results [8], when the transformation rate is normalized with respect to the nuclear stopping component of the ion energy loss. Fig. 9 shows the transformation percentage (t%) for Ne^+ versus Kr^+ ion irradiation as a function of dpa (Ne^+ results from Fig. 8; Kr^+ results from Ref. [8]). These results indicate that m-ZrO_2 exhibits a sensitivity to irradiation spectrum. Fig. 10 shows how the electronic-to-nuclear stopping power (ENSP) ratio varies as a function of depth in a ZrO_2 target for 150 keV Ne^+ versus 300 keV Kr^{++} ions (based on

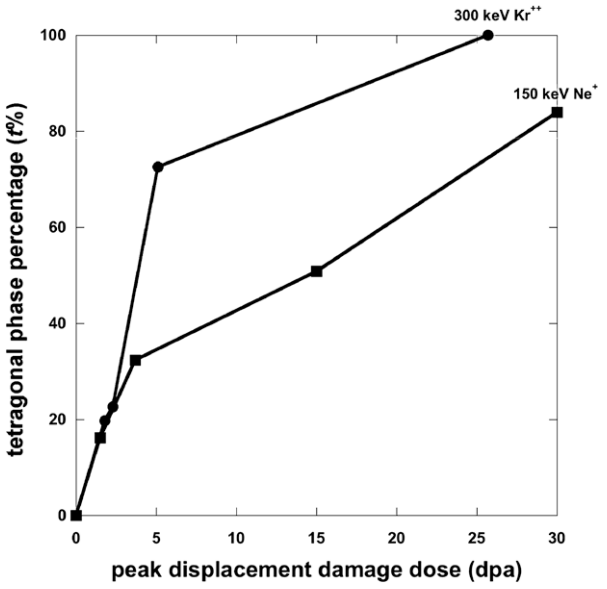

Fig. 9. Tetragonal (t) phase evolution as a function of displacement damage dose for 150 keV Ne^+ versus 300 keV Kr^{++} ion irradiations of ZrO_2. These results are based on GIXRD measurements of Ne^+ ion irradiated samples from this study and on Kr^{++} ion irradiated samples from Valdez et al. [8].

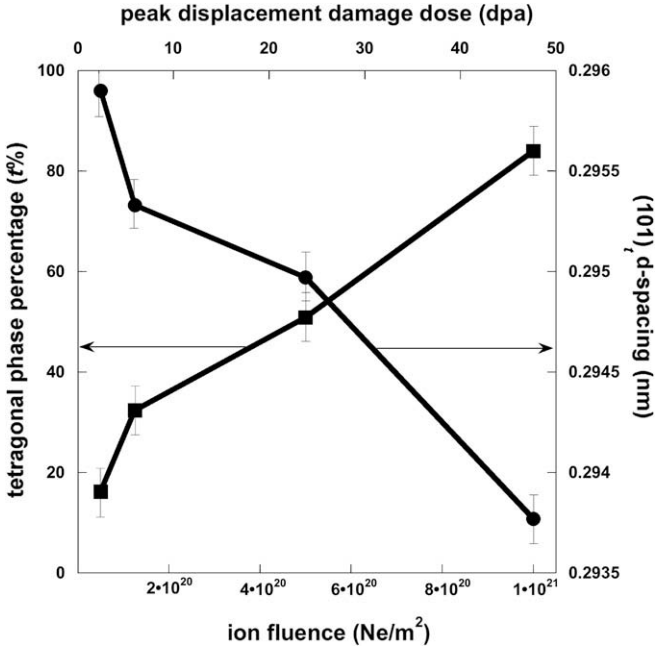

Fig. 8. ZrO_2 tetragonal (t) phase evolution and evolution of the d-spacing belonging to the $(101)_t$ family of t-ZrO_2 planes, as a function Ne^+ ion fluence. These results are based on GIXRD measurements using an X-ray incidence angle, of $\gamma = 0.25°$ (see text for discussion).

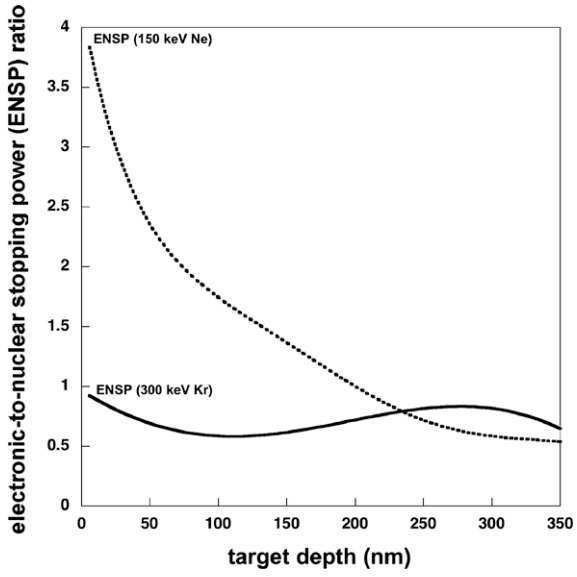

Fig. 10. SRIM simulation results comparing the electronic-to-nuclear stopping power (ENSP) ratio for 150 keV Ne^+ versus 300 keV Kr^{++} ion irradiated of ZrO_2 as a function of depth. The variation in ENSP as a function of depth for the 300 keV Kr^{++} ions is not statistically significant (the uncertainty in ENSP is ±0.25).

SRIM-2000 ion stopping simulations). Fig. 10 indicates that ENSP is significantly larger for 150 keV Ne^+ ions compared to 300 keV Kr^+ ions throughout most of the range of both ions. ENSP for 150 keV Ne^+ ions exhibits a maximum of ~4.5 near the sample surface and is greater than 1 to a depth of ~200 nm. On the contrary, ENSP for 300 keV Kr^+ ions is less than 1 over the entire ion range. One explanation for the more sluggish *m–t* transformation rate observed for Ne^+ ion irradiations may be that the greater ionization loss per unit damage energy leads to enhanced ionization-induced point defect diffusion, which in turn promotes recombination of the defects responsible for the *m–t* transformation.

In accordance with typical materials behavior under irradiation, the ion irradiation-induced phase transformation of zirconia described here involves a transition to a structure of higher crystal symmetry (tetragonal versus monoclinic). Somewhat surprisingly, however, radiation damage studies of zirconia thus far have failed to reveal a transformation to the highest symmetry polymorph of zirconia, the cubic fluorite phase. So, even though unstabilized zirconia has proven highly resistant to amorphization, it manages this without adopting the structure of the highest symmetry polymorph of ZrO_2, the isometric cubic structure. On the contrary, a crystalline asymmetry persists in irradiated zirconia to very high levels of radiation damage. The prediction by Sickafus et al. [24] of a transformation to the cubic, fluorite-structured phase of zirconia is not realized under the radiation damage conditions presented here. Nevertheless, it still seems plausible that an *m–t–c* transformation may occur at higher ion doses, as we find that the *t*-ZrO_2 molecular volume continues to contract with increasing ion fluence.

It is interesting that irradiation produces a tetragonal phase with a higher density than that of the parent monoclinic phase. Comparing pristine *m*-ZrO_2 with irradiation-induced *t*-ZrO_2, we find that the volume per molecule of ZrO_2 decreases from .0352 to .0329 nm^3 upon undergoing the irradiation-induced *m-t* transformation (the value for *t*-ZrO_2 is for the highest ion irradiation dose used in these experiments). This represents approximately a 6.5% increase in density for this irradiation-induced transformation. This density increase may be compared with density differences for *m*-ZrO_2 [16] and low temperature metastable *t*-ZrO_2 [21], which differ in density by ~5.6% (*t*-ZrO_2 being the higher). The density increase observed here was also observed in our previous investigation of irradiation effects in *m*-ZrO_2 using 300 keV Kr^{++} ions [8]. Interestingly, we also recently observed an increase in density upon phase transformation in Kr^{++} ion irradiated Dy_2O_3 [25]. It should be noted that fused (vitreous) silica densifies during irradiation near room temperature to form a higher density amorphous silica phase [26], but the lattice contraction observations described above may be the first observations of such behavior in crystalline solids during irradiation.

It is also well known from detailed studies of the crystallography of the various polymorphs of zirconia that the *m–t* transformation is accompanied by an increase in coordination of the Zr atoms from 7- to 8-fold (see, e.g., Ref. [27]). This also would seem a surprising materials' response to irradiation, although the effect is not unprecedented. The irradiation-induced phase transformation we observed previously in the sesquioxide dysprosia, Dy_2O_3, shares a similar characteristic [25]: namely, an increase in cation coordination upon irradiation from 6-fold to a mixture of 6- and 7-fold.

A final consideration for discussion is the possibility for experimental artifacts associated with near-surface ion implantation. First is the possibility that the lattice contraction we observed with increasing ion dose may be due to implanted ions. We believe this should not be the case since the implanted Ne ions should promote lattice expansion, not shrinkage. The second possibility is that the *m–t* transformation observed here could be due to compressive lattice stress in the irradiated region, associated with the high concentration of implanted Ne ions (up to 6 at.% Ne for the highest dose (Fig. 2)). It has already been shown that stress can increase dramatically with increasing implanted ion concentration (see, e.g., Ref. [28]). But if the transformation we observe is stress-induced, we might expect a high-pressure polymorph of zirconia to emerge with increasing dose, rather than a high-temperature polymorph. Of the known high-pressure phases of zirconia, three (and perhaps a fourth) are orthorhombic [29], while there is some controversy about an additional tetragonal phase [30]. However, the latter phase was determined to have lattice parameters and symmetry elements far different from the tetragonal phase we observed in this study. Nevertheless, since these high-pressure phases may be kinetically inhibited from forming under our cryogenic irradiation conditions, a stress-induced mechanism for the *m–t* transformation cannot be ruled out.

5. Summary

Polycrystalline samples of monoclinic zirconia (specifically, $ZrO_{1.98}$) were irradiated at cryogenic temperature (~80 K) with 150 keV Ne^+ ions over a range of ion fluences from 5×10^{19} to 1×10^{21} Ne/m^2 (this fluence range corresponds to peak displacement damage doses ranging from 2 to 44 dpa). Transmission electron microscopy observations revealed that at an ion fluence of 5×10^{20} Ne/m^2, the buried irradiated region was completely transformed from a monoclinic (*m*) structure to a tetragonal (*t*) structure of ZrO_2, while the upper, near-surface irradiated region consisted of a mixture of *m* and *t*-phases. Grazing incidence X-ray diffraction measurements were used to estimate the percentage of *t*-phase produced by ion irradiation. It was found that at the highest ion fluence of 1×10^{21} Ne/m^2, the irradiated zirconia was approximately 85% transformed to the *t*-phase. The irradiation-induced transformation rate observed here is somewhat more sluggish than the rate observed in previous experiments using 300 keV Kr^{++} irradiating ions [8], when the transformation rate is normalized in terms of the nuclear energy deposition. This suggests that electronic and nuclear stopping both play a role in the *m–t* transformation and in recovery to the *m*-phase. The X-ray diffraction measurements also revealed that a significant increase in density (~6.5%) accompanies the *m–t* irradiation-induced transformation. Raman spectroscopy also provided evidence for the *m–t* irradiation-induced transformation. Finally, it is worth noting that in this study, no evidence was found for transformation to the cubic (*c*) phase, nor was any amorphization transformation observed.

Acknowledgements

This work was sponsored by the US Department of Energy, Office of Basic Energy Sciences, Division of Materials Sciences and Engineering.

References

[1] W.M. Kriven, W.L. Fraser, S.W. Kennedy, Martensite crystallography of tetragonal zirconia, in: A.H. Heuer, L.W. Hobbs (Eds.), Science and Technology of Zirconia, Advances in Ceramics, The American Ceramic Society, Inc, Columbus, OH, 1981, p. 82.
[2] E.C. Subbarao, Zirconia an overview, in: A.H. Heuer, L.W. Hobbs (Eds.), Science and Technology of Zirconia, Advances in Ceramics, The American Ceramic Society, Inc, Columbus, OH, 1981, p. 1.
[3] A.G. Evans, Toughening mechanisms in zirconia alloys, in: N. Claussen, M. Rühle, A.H. Heuer (Eds.), Science and Technology of Zirconia II, Advances in Ceramics, The American Ceramic Society, Inc, Columbus, OH, 1984, p. 193.
[4] G. Teufer, Acta Cryst. 15 (1962) 1187.
[5] K.E. Sickafus, H. Matzke, T. Hartmann, K. Yasuda, J.A. Valdez, P. Chodak III, M. Nastasi, R.A. Verrall, J. Nucl. Mater. 274 (1999) 66.
[6] I.V. Afanasyev-Charkin, K.E. Sickafus, J. Nucl. Mater. 306 (2–3) (2002) 112.
[7] D. Simeone, J.L. Bechade, D. Gosset, A. Chevarier, P. Daniel, H. Pilliaire, G. Baldinozzi, J. Nucl. Mater. 281 (2000) 171.

[8] J.A. Valdez, M. Tang, C. Zhenhuan, M.I. Peters, K.E. Sickafus, Nucl. Instrum. and Meth. B 218 (2004) 103.
[9] A. Benyagoub, F. Levesque, F. Couvreur, C. Gibert-Mougel, C. Dufour, E. Paumier, Appl. Phys. Lett. 77 (20) (2000) 3197.
[10] A. Benyagoub, F. Couvreur, S. Bouffard, F. Levesque, C. Dufour, E. Paumier, Nucl. Instrum. and Meth. B 175–177 (2001) 417.
[11] A. Benyagoub, Nucl. Instrum. and Meth. B 206 (2003) 132.
[12] S.J. Zinkle, Nucl. Instrum. and Meth. B 91 (1994) 234.
[13] S.J. Zinkle, J. Nucl. Mater. 219 (1995) 113.
[14] S.J. Zinkle, Mater. Res. Soc. Symp. Proc. 373 (1995) 287.
[15] S.J. Zinkle, Mater. Res. Soc. Symp. Proc. 439 (1997) 667.
[16] C.J. Howard, R.J. Hill, B.E. Reichert, Acta Cryst. B 44 (1988) 116.
[17] Joint Committee for Powder Diffraction Studies – International Centre for Diffraction Data (JCPDS ICDD), Powder Diffraction File™, Release 2000.
[18] J.F. Ziegler, J.P. Biersack, U. Littmark, in: J.F. Ziegler (Ed.), The Stopping and Range of Ions in Solids, Pergamon Press, New York, 1985.
[19] D. Rafaja, V. Valvoda, Vaclav A.J. Perry, J.R. Treglio, Surf. Coat. Technol. 92 (1997) 135.
[20] A. Guinier, X-Ray Diffraction in Crystals, Imperfect Crystals and Amorphous Bodies, Dover Publications, Inc, New York, 1994.
[21] G. Lim, W. Parrish, C. Ortiz, M. Bellotto, M. Hart, J. Mater. Res. 2 (1987) 471.
[22] J. Málek, L. Benes, T. Mitsuhashi, Powder Diff. 12 (2) (1997) 96.
[23] R.C. Garvie, P.S. Nicholson, J. Am. Ceram. Soc. 55 (1972) 300.
[24] K.E. Sickafus, J.A. Valdez, J.R. Williams, R.W. Grimes, H.T. Hawkins, Nucl. Instrum. and Meth. B 191 (2002) 549.
[25] M. Tang, J.A. Valdez, P. Lu, G.E. Gosnell, C.J. Wetteland, K.E. Sickafus, J. Nucl. Mater. 328 (2004) 71.
[26] F.W. Clinard Jr., L.W. Hobbs, in: R.A. Johnson, A.N. Orlov (Eds.), Physics of Radiation Effects in Crystals, Elsevier, Amsterdam, 1986, p. 387.
[27] D.J. Green, R.H.J. Hannink, M.V. Swain, Transformation Toughening of Ceramics, CRC Press, Boca Raton, Florida, 1989.
[28] A. Misra, S. Fayeulle, H. Kung, T.E. Mitchell, M. Nastasi, Nucl. Instrum. and Meth. B 148 (1999) 211.
[29] J.M. Leger, P.E. Tomaszewski, A. Atouf, A.S. Pereira, Phys. Rev. B 47 (21) (1993) 14075.
[30] H. Arashi, T. Yagi, S. Akimoto, Y. Kudoh, Phys. Rev. B 41 (7) (1990) 4309.